# $Pr_2Ir_2O_7$: When Luttinger Semimetal Meets Melko-Hertog-Gingras Spin Ice State

Xu-Ping Yao[1,2] and Gang Chen[1,2,3,4,*]

[1]*State Key Laboratory of Surface Physics and Department of Physics, Fudan University, Shanghai 200433, China*

[2]*Center for Field Theory and Particle Physics, Fudan University, Shanghai 200433, China*

[3]*Institute for Nanoelectronic Devices and Quantum Computing, Fudan University, Shanghai 200433, China*

[4]*Collaborative Innovation Center of Advanced Microstructures, Nanjing University, Nanjing 210093, China*

(Received 22 December 2017; revised manuscript received 4 July 2018; published 4 December 2018)

In quantum materials with multiple degrees of freedom such as itinerant electrons and local moments, the interplay between them leads to intriguing phenomena and allows the mutual control of each other. Here, we study band topology and engineering from the interplay between local moments and itinerant electrons in pyrochlore iridates. For metallic $Pr_2Ir_2O_7$, the Ir $5d$ conduction electrons interact with the Pr $4f$ local moments via the $f$-$d$ exchange. While the Ir electrons form a Luttinger semimetal, the Pr moments can be tuned into an ordered spin ice with a finite ordering wave vector, dubbed the Melko-Hertog-Gingras state, by varying Ir and O contents. We point out that the Pr Ising order generates an internal field and reconstructs the Ir bands. Besides the broad existence of Weyl nodes, we predict that the magnetic translation of the Pr Melko-Hertog-Gingras state protects the Dirac-band touching at certain time-reversal invariant momenta for the Ir electrons. We propose the magnetic fields to control the Pr magnetism and thereby indirectly influence the Ir conduction electrons. Our prediction can be immediately tested in ordered $Pr_2 Ir_2O_7$ samples. Our theory should stimulate experiments on pyrochlore iridates, constitute a nontrivial and realistic example for the interplay between itinerant electrons and local moments in three dimensions, and shed light on hybrid quantum materials with multiple degrees of freedom.

DOI: 10.1103/PhysRevX.8.041039

Subject Areas: Condensed Matter Physics, Materials Science, Strongly Correlated Materials

## I. INTRODUCTION

The study of the electron band-structure topology has attracted a significant attention since the proposal and discovery of topological insulators [1–4]. The fundamental aspect between the topological protection and the band structure has been well understood theoretically. More practically, there is a growing effort that proposes experimental schemes such as the strain or magnetic dopings to control or engineer the band-structure topology. Along this line, a great success was achieved in the discovery of the quantum anomalous Hall effect in the magnetically doped $Bi_2Se_3$ materials [5–7]. Over there, the surface Dirac electron of the topological insulator obtains a mass gap from the simple ferromagnetically ordered dopants, and the resulting valence band develops a nontrivial Chern number and supports a chiral edge state for the quantized Hall transport. These two ingredients, i.e., itinerant electrons with a Dirac spectrum and the ferromagnetic local moments, simple on their own, together generate the remarkable phenomenon of the quantum anomalous Hall effect. Therefore, quantum materials that contain extra degrees of freedom (d.o.f.) besides the nearly free electrons, would be ideal for the practical purpose to control the band-structure properties and produce nontrivial phenomena.

In this work, we study the Pr-based pyrochlore iridate where the Pr ions provide local moments and the Ir ions give the itinerant electrons. We show that the $4f$ local moments of the Pr ions and their impacts on the Ir itinerant electrons provide a *natural setup* to explore the band-structure engineering via the coupling between these two distinct d.o.f. Pyrochlore iridates $R_2Ir_2O_7$ have received considerable attention in recent years partly because the $5d$ electrons of the Ir subsystem provide an interesting arena to explore the correlation effects in the strong spin-orbit-coupled matters [8–10]. Aligned with this original motivation, many interesting phases and phenomena, including

*gangchen.physics@gmail.com

topological band insulator [8,11], topological Mott insulator [8,12], axion insulator [13,14], Weyl semimetal [13–16], Luttinger-Abrikosov-Beneslavskii non-Fermi liquid [17], and others, have been proposed [11,13–22]. Despite the fruitful achievements under the original motivation [23–30], the role of the rare-earth local moments in these systems has not been extensively studied except few works [14,18,31]. Recent experiments [32,33] in $Nd_2Ir_2O_7$ and $Pr_2Ir_2O_7$ do suggest the importance of the rare-earth local moments and the coupling between the local moments and the itinerant electrons.

Our work is mainly inspired by the experiments on $Pr_2Ir_2O_7$. Depending on the stoichiometry, the $Pr_2Ir_2O_7$ samples show rather different behaviors. While the early samples remain metallic and paramagnetic down to the lowest temperatures [33–35], recent samples with different iridium and oxygen contents develop an antiferromagnetic Ising order in the Pr subsystem with a $2\pi(001)$ ordering wave vector [36]. This particular order is a state within the "2-in–2-out" spin ice manifold and coincides with the classical spin ground state of classical dipolar spin model on the pyrochlore lattice that was numerically found by Melko, Hertog, and Gingras in Ref. [37]. Although the physical origin of this order in $Pr_2Ir_2O_7$ differs from the classical and dipolar interaction in Ref. [37], we refer this Ising order as "Melko-Hertog-Gingras" (MHG) spin ice state or order. Since the Pr local moment was argued to fluctuate within the 2-in–2-out spin ice manifold in the paramagnetic samples and the MHG state of the ordered samples is a particular antiferromagnetic state within the spin ice manifold [38–40], it was proposed by one of us that, the Pr subsystem is proximate to a quantum phase transition from the $U(1)$ quantum spin liquid to the MHG order via a confinement transition by proliferating the "magnetic monopoles" [41].

Besides the interesting aspects of the Pr local moments, the Ir conduction electron was shown to display interesting phenomena. Recent works have identified the presence of a quadratic band touching at the $\Gamma$ point for the Ir $5d$ electrons [42–44]. This semimetallic state with a quadratic band touching is thus quoted as "Luttinger semimetal." Theoretical works have considered the long-range Coulomb interaction for the Luttinger semimetal phase of the Ir subsystem [17]. These efforts surely fall into the original motivation of searching for correlation physics in strong spin-orbit-coupled matter [8,20] and provide an important understanding of the rich physics in this material. The purpose of our work here is to deviate from the intense efforts on the correlation physics of the Ir subsystems, and is instead to understand the interplay between the Ir conduction electrons and the Pr local moments. As it has already been pointed out in Ref. [41], the large and finite ordering wave vector of the Pr local moments and the quadratic band touching of the Ir $5d$ electrons suppress the Yukawa coupling between the Pr magnetic order and the Ir particle-hole excitation near the (small) Fermi surface or $\Gamma$ point because the large and finite ordering wave vector connects the $\Gamma$ point to the Ir bands without states near the Fermi energy. Therefore, the Ir electron near the Fermi surface does not modify the critical and long-distance properties of the Pr local moments at the lowest order, though it is thought that the phase transition of the Pr local moment was induced by the modified Ruderman-Kittel-Kasuya-Yosida (RKKY) interaction mediated by the Ir electrons [41]. The opposite, however, is not true. The Luttinger semimetal with a quadratic band touching is a parent state of various topological phases such as Weyl semimetal and topological insulator [42,45,46]. The coupling to the Pr local moment naturally provides such a perturbation to the Luttinger semimetal. In this work, we focus on the Ising ordered phase of the Pr subsystem and explain the effect of the Pr magnetism on the Ir conduction electrons.

In $Eu_2Ir_2O_7$ and other pyrochlore iridates [24,25,32], the Ir subsystem experiences a metal-insulator transition by developing an all-in all-out magnetic order with the ordering wave vector $\boldsymbol{Q} = \boldsymbol{0}$, and it is believed that the magnetic order is driven by the correlation of the Ir $5d$ electrons. For $Pr_2Ir_2O_7$, the magnetic unit cell of $Pr_2Ir_2O_7$ is twice the size of the crystal unit cell, and it is the Pr local moment that develops the magnetic order. The exchange field, that is experienced by the Ir conduction electron and generated by the MHG order of Pr moments, is thus very different from other pyrochlore iridates. Therefore, we construct a minimal model to incorporate the coupling and interactions of the relevant microscopic d.o.f. This model, as we introduce in Sec. II, naturally captures the physics that we describe above. We find that the exchange field enlarges the unit cell of the Ir subsystems, and couples the electrons and holes near the $\Gamma$ point with the electrons and holes near the ordering wave vector $\boldsymbol{Q} = 2\pi(001)$. The combination of the time-reversal operation and the elementary lattice translation by $(1/2, 0, 1/2)$ or $(0, 1/2, 1/2)$ remains to be an (antiunitary) symmetry of the MHG state. Using this symmetry, we demonstrate that there exist Dirac-band touchings at the high symmetry momenta. Our explicit calculation with the realistic model confirms these band touchings. In addition, we find the existence of Weyl nodes in the Ir band structure due to the breaking of the time-reversal symmetry by the Pr magnetic order. Unlike the symmetry-protected Dirac-band touchings, the Weyl nodes are not symmetry protected and are instead topologically stable.

Apart from the immediate effect on the Ir conduction electron from the Pr Ising magnetic order, we further explore the role of the external magnetic field. It is noticed that the external magnetic field primarily couples to the Pr local moments rather than to the conduction electron. This is because every Pr local moment couples to the external magnetic field, while for the Ir conduction electrons only small amount of electrons on the Fermi surface couple to

the magnetic field, not to say, there is a vanishing density of states if the Fermi energy sits right at the Γ point of the quadratic band touching. The Zeeman coupling to the Pr local moment would simply favor a $\boldsymbol{Q} = \boldsymbol{0}$ state and thus competes with the exchange interaction of the Pr subsystem. The combination of the magnetic field and the Pr exchange coupling generates several different magnetic states for the Pr local moments. These magnetic orders create distinct exchange fields on the Ir conduction electrons and thereby gives new types of reconstructions of the conduction electron bands. From the symmetry point of view, the Dirac-band touchings at the time-reversal invariant momenta are no longer present in the magnetic field. We further find that the Weyl nodes exist broadly when the magnetic field is applied to the system. This provides a feasible experimental scheme to engineer the band-structure properties of the Ir itinerant electrons.

The remaining parts of the paper are organized as follows. In Sec. II, we introduce the microscopic Hamiltonian for the Ir subsystem and the $f$-$d$ exchange between the Ir subsystem and the Pr subsystem. In Sec. III, we include the antiferromagnetic Ising order of the Pr local moments and study the reconstruction of the Ir band structure under this magnetic order. In Sec. IV, we further explore the interplay between the Zeeman coupling, the Pr exchange coupling, and the Ir band structure, and point out that the external field can be used to engineer the topological band structure. Finally, in Sec. V, we propose various experiments to confirm our prediction and suggest the application and impact to the hybrid quantum materials with both itinerant electrons and local moments.

## II. MICROSCOPIC MODEL

We here propose the minimal microscopic model for $Pr_2Ir_2O_7$ and explain the limitation of the model. The approximation in the minimal model is further justified and designed to reveal the physics that we discuss in this paper. The full Hamiltonian of this system should contain the following ingredients [14],

$$H = H_{\mathrm{TB}} + H_{\mathrm{ex}} + H_{\mathrm{fd}} + H_{\mathrm{Zeeman}}, \tag{1}$$

where $H_{\mathrm{TB}}$ is the tight-binding model of the Ir conduction electron, $H_{\mathrm{ex}}$ is the interaction between the Pr local moments and originates from the superexchange process and the dipolar interaction, $H_{\mathrm{fd}}$ is the coupling between the Pr local moment with the spin density of the Ir conduction electrons, and the $H_{\mathrm{Zeeman}}$ defines the Zeeman coupling of the Pr local moment to the external magnetic field.

### A. Ir subsystem

We start with the tight-binding model for the Ir conduction electrons. The $Ir^{4+}$ ion has a $5d^5$ electron configuration, and these five electrons occupy the $t_{2g}$ orbitals.

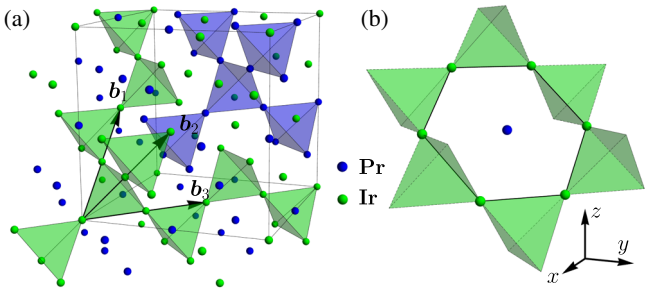


FIG. 1. The pyrochlore lattice structure for $Pr_2Ir_2O_7$. (a) Both Ir and Pr ions form pyrochlore lattices of corner-sharing tetrahedra. (b) For each Pr ion, six nearest Ir ions form a hexagon with the Pr ion in the hexagon center.

The atomic spin-orbit coupling splits the sixfold degenerate spin and orbital states in the $t_{2g}$ manifold into the lower $j = 3/2$ quadruplets and the upper $j = 1/2$ doublets. Because of the lattice geometry of the pyrochlore system, the $t_{2g}$ orbitals and the effective spin $\boldsymbol{J}$ are defined in the local coordinate system of the $IrO_6$ octahedron. For the $Ir^{4+}$ ion, the lower $j = 3/2$ quadruplets are fully filled, and the upper $j = 1/2$ doublets are half filled [8,47–49]. It was shown that the pyrochlore iridate band structure near the Fermi level is well approximated by a tight-binding model based on the $j = 1/2$ doublets [8,11,16,42]. The model is given as

$$H_{\mathrm{TB}} = \sum_{i,j\in\mathrm{Ir}} \sum_{\alpha\beta} t_{ij,\alpha\beta} d^{\dagger}_{i\alpha} d_{j\beta}, \tag{2}$$

where $d^{\dagger}_{i\alpha}$ ($d_{i\alpha}$) creates (annihilates) an electron with an effective spin $\alpha$ in the $j = 1/2$ doublet. The hopping $t_{ij,\alpha\beta}$ includes both the direct electron hoppings ($t_\sigma$ and $t_\pi$) between the nearest-neighbor Ir ions and the indirect electron hopping ($t_{\mathrm{id}}$) through the intermediate oxygen. It has been shown [16] that in the regime $-1.67t_{\mathrm{id}} < t_\sigma < -0.67t_{\mathrm{id}}$ and $t_\pi = -2t_\sigma/3$, the system becomes a Luttinger semimetal with a quadratic band touching at the Γ point. This quadratic band touching is protected by the cubic lattice symmetry [11,42,43]. The Ir conduction electron of $Pr_2Ir_2O_7$ is described by the Luttinger semimetal of this tight-binding model.

In contrast to other pyrochlore iridates, $Pr_2Ir_2O_7$ is experimentally known to be metallic [9,10], so the Hubbard-$U$ for the Ir atoms is apparently insufficient to drive a Mott transition. Therefore, while Hubbard-$U$ is certainly necessary to understand the correlation physics and/or Mott transition of pyrochlore iridates, in this work we will assume it can be accounted for through a renormalization of the band-structure parameters, which we treat as phenomenological parameters to obtain a phase diagram. The quadratic band touching at Γ point and the emergence of Dirac and Weyl band touchings are robust against the moderate Hubbard-$U$. Indeed, density functional theory

calculation without Hubbard-$U$ finds a larger bandwidth than the experimental bandwidth whose suppression is due to the electron correlation [42]. Without losing any generality [16], we follow Kim's group by setting $t_\pi = -2t_\sigma/3$, and we further set $t_{\rm id} = -t_\sigma$ throughout this work.

Prior theoretical works, that focused on the Ir subsystem, have invoked the k.p theory and the Luttinger model as the starting point to analyze the correlation effect of the electrons [17,19,50–56]. In our case, the MHG spin ice state of the Pr local moments has a large and finite ordering wave vector and necessarily connect the Ir bands near the Γ point with the bands near the ordering wave vector, so the lattice effects cannot be ignored. As a result, we cannot start with the k.p theory of the Γ point at low energies. Instead, we should either include the band-structure information near both the Γ point and the ordering wave vector or directly start from the lattice model. In this work, we rely on the lattice model and start with the tight-binding model for the Ir subsystem.

### B. Pr subsystem

The $Pr^{3+}$ ion has a $4f^2$ electron configuration, and the $4f$ electron is well localized. The combination of the atomic spin-orbit coupling and the crystal electric field creates a twofold degenerate ground state for the $Pr^{3+}$ ion. This twofold ground-state degeneracy defines the non-Kramers doublet nature of the Pr local moment, and a pseudospin-1/2 operator $\boldsymbol{\tau}_i$ is introduced to operate on the twofold degenerate ground states. The non-Kramers doublet has a peculiar property under the time-reversal symmetry, i.e.,

$$\mathcal{T}:\ \tau_i^z \to -\tau_i^z, \tag{3}$$

$$\mathcal{T}:\ \tau_i^x \to +\tau_i^x, \tag{4}$$

$$\mathcal{T}:\ \tau_i^y \to +\tau_i^y, \tag{5}$$

where the $z$ direction is defined locally on each sublattice and is given as the local (111) lattice direction of the pyrochlore system. Here, the magnetic dipolar moment is purely from the $\tau^z$ component, and the transverse components are known to be the quadrupolar moments.

Because of the spin-orbit-entangled nature of the Pr local moment, the effective interaction between the Pr local moments is anisotropic in the pseudospin space and also depends on the bond orientation. The general form of the interaction is [57–59]

$$\tilde{H}_{\rm ex} = \sum_{ij} J_{z,ij}\tau_i^z\tau_j^z + \sum_{ij} J_{\perp,ij} \sum_{\mu,\nu=x,y} \tau_i^\mu \tau_j^\nu, \tag{6}$$

where the interaction between the Ising component $\tau^z$ and the transverse component $\tau^{x,y}$ is strictly forbidden by time-reversal symmetry. Here, $\tilde{H}_{\rm ex}$ differs from $H_{\rm ex}$ in Eq. (1). $\tilde{H}_{\rm ex}$ contains all sources of interactions between the local moments, and is obtained by integrating out the Ir conduction electrons. $\tilde{H}_{\rm ex}$ would contain both the RKKY interaction and $H_{\rm ex}$. Since the Pr local moment is in the spin ice manifold, we thus expect the nearest-neighbor Ising interaction $J_{z,ij}$ is positive and dominant. The interaction between the transverse components creates the quantum fluctuation so that the system fluctuates quantum mechanically within the spin ice manifold. Clearly, the nearest-neighbor interaction alone cannot generate the finite momentum Ising order of the Pr subsystem whose magnetic unit cell is twice the size of the crystal unit cell. Further neighbor interactions are required. We here introduce the third neighbor antiferromagnetic Ising interaction and approximate $\tilde{H}_{\rm ex}$ as

$$\tilde{H}_{\rm ex} \simeq \sum_{\langle ij\rangle} J_{1z}\tau_i^z\tau_j^z + \sum_{\langle\langle\langle ij\rangle\rangle\rangle} J_{3z}\tau_i^z\tau_j^z, \tag{7}$$

where the interaction between the transverse components has been abandoned in this approximation. In our previous work [41] that focuses on the quantum phase transition of the Pr subsystem, this quantum fluctuation is an important ingredient to understand the nature of the phase transition and the nearby phases. In contrast, our purpose in this paper is to understand the feedback effect on the Ir electron structure from the Pr Ising magnetic order, so the quantum dynamics of the Pr local moment is irrelevant for this purpose. In Sec. III of the paper, we would simply regard the Ising magnetic order that is observed in $Pr_2Ir_2O_7$ as a given condition, and this exchange Hamiltonian is not invoked until in Sec. IV where the external Zeeman coupling competes with the exchange and modifies the Pr magnetic order.

The extended interaction for the Pr local moments in $Pr_2Ir_2O_7$ is expected because the RKKY interaction that is mediated by the Ir conduction electrons is not short ranged. This is quite different from the usual rare-earth magnets where the exchange interaction is often short ranged and mostly restricted to the nearest neighbors [60]. The long-range or extended RKKY interaction is the reason that we point out the Ir conduction drives the quantum phase transition of the Pr moments.

Because of the Ising nature of the moment in the approximate exchange model, the ground state is antiferromagnetically ordered with an ordering wave vector $\boldsymbol{Q} = 2\pi(001)$ for $J_{3z} > 0$. Clearly, the approximate model captures the observed magnetic order in $Pr_2Ir_2O_7$.

### C. Pr-Ir coupling

Precisely because of the non-Kramers doublet nature of the Pr local moment, it was pointed out in Ref. [14] based on the space group symmetry analysis that, the $\tau^z$ component couples to the spin density of the Ir conduction electron while the transverse component would couple to the electron density. The transverse component may also couple to the spin current that is even under time reversal

[14]. The general expression for the $f$-$d$ exchange between the Pr local moment and the Ir spin density has been obtained in the previous work [14]. The coupling between the transverse component $\tau^{x,y}$ and the Ir electron density was worked out in Ref. [18]. Again, since it is the Ising component $\tau^z$ of the Pr local moment that develops the magnetic order in $Pr_2Ir_2O_7$, the leading order effect on the Ir conduction electron originates from the coupling between the Ir spin density and the Pr Ising component. Therefore, we consider the following $f$-$d$ exchange between the Pr Ising moment and the Ir spin density [14]

$$H_{\rm fd} = \sum_{\langle ij\rangle}\sum_{i\in \rm Pr}\sum_{j\in \rm Ir}\tau_i^z\left[\left(d_{j\alpha}^\dagger \frac{\boldsymbol{\sigma}_{\alpha\beta}}{2} d_{j\beta}\right)\cdot \boldsymbol{v}_{ij}\right], \tag{8}$$

where $\boldsymbol{v}_{ij}$ is a vector that defines the coupling between the Ir spin density and the Pr local moments. For each Pr ion, there are six Ir ions nearby, and these six Ir ions form a hexagon with the Pr ion in the hexagon center (see Fig. 1). Under the nearest-neighbor Kondo-like coupling approximation, the standard symmetry analysis gives, e.g.,

$$v_{11} = (0,0,0), \tag{9}$$

$$v_{12} = (c_1, c_2, c_2), \tag{10}$$

$$v_{13} = (c_2, c_1, c_2), \tag{11}$$

$$v_{14} = (c_2, c_2, c_1), \tag{12}$$

where $c_1$, $c_2$ are the two $f$-$d$ exchange parameters, and other $\boldsymbol{v}_{ij}$'s can be obtained by simple lattice symmetry operations [14]. The choices of the Pr and Ir sublattices are defined in Appendix A.

### D. Zeeman coupling

Finally, we introduce the Zeeman coupling. Because only the $\tau^z$ is odd under time reversal, we have the Zeeman coupling

$$\begin{aligned} H_{\rm Zeeman} &= -g\mu_B B\sum_{i\in \rm Pr}\tau_i^z(\hat{z}_i\cdot\hat{n}),\\ &\equiv -h\sum_{i\in \rm Pr}\tau_i^z(\hat{z}_i\cdot\hat{n}), \end{aligned} \tag{13}$$

where $\hat{n}$ is the direction of the external magnetic field. The $\hat{z}_i$ direction is defined locally for each sublattice of the Pr subsystem.

### E. Energy scales

Clearly, the largest energy scale in the model is the bandwidth and interaction of the Ir conduction electrons. The second largest energy scale is the $f$-$d$ exchange coupling. The lowest ones would be the exchange coupling between the Pr moments and the Zeeman coupling. Since the Zeeman coupling can be tuned experimentally, the magnetic state of the Pr local moments can thus be manipulated by the external magnetic field. As the rare-earth local moments such as Pr moments here interact with a rather small energy scale, a magnetic field in the laboratory setting could achieve the goal.

## III. DIRAC-BAND TOUCHINGS AND WEYL NODES OF THE IRIDIUM SUBSYSTEM

For $Pr_2Ir_2O_7$, the Ir conduction electrons were found to develop a Luttinger semimetallic band structure that is similar to the bulk HgTe [42–46]. It is well known that the Luttinger semimetal is a parent state of various topological phases such as topological insulator and Weyl semimetal [42,45,46]. The Pr Ising order breaks the time-reversal symmetry, and the time-reversal symmetry breaking is transmitted to the Luttinger semimetal of the Ir subsystem through the $f$-$d$ exchange. We here study the band-structure reconstruction of the Ir $5d$ electrons through the above mechanism.

### A. Emergent Dirac-band touchings

The Pr local moments were found to develop the MHG spin ice state in the recent samples with different Ir and O contents from the old ones [36]. The MHG spin ice state breaks the time-reversal symmetry and the lattice translation by doubling the crystal unit cell. Because of this interesting magnetic-ordering structure, the combination of the time reversal and certain lattice translations remains to be a symmetry of the system after the development of the Ising magnetic ordering. As we show below, this symmetry leads to a remarkable band-structure property of the Ir subsystem after the band reconstruction.

The reconstructed band structure of the Ir conduction electrons is governed by the Ir tight-binding model and the $f$-$d$ exchange, $H_{\rm TB} + H_{\rm fd}$. As a comparison, we first evaluate the Ir band structure in the magnetic Brillouin zone corresponding to the doubled unit cell due to the Pr Ising magnetic order. As we depict in Fig. 2, the Ir conduction electron bands form a Luttinger semimetal in the *absence* of the Pr magnetic order and give a quadratic band touching at the $\tilde{\Gamma}$ point. Without losing any generality, in Fig. 2 we choose the MHG spin ice state of the Pr moments to have a propagating wave vector $\boldsymbol{Q} = 2\pi(001)$ and the band structure in Fig. 2(d) is plotted in the magnetic Brillouin zone of Fig. 2(b). Before the appearance of the Pr Ising order, the system has both time reversal ($\mathcal{T}$) and inversion ($\mathcal{I}$) symmetries, and each band of the Ir electrons has a twofold Kramers degeneracy. The quadratic band touching at the $\tilde{\Gamma}$ point results from the cubic symmetry. As the Pr Ising magnetic order appears, the Ir band structure is immediately modified. Before we present the reconstructed band structure in detail, we first understand

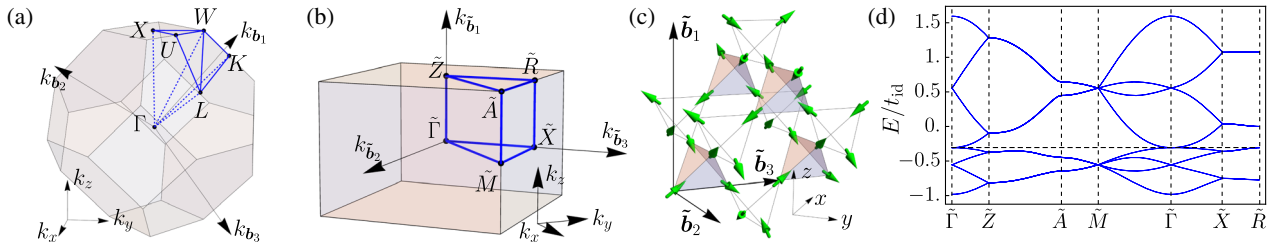


FIG. 2. (a) The (crystal) Brillouin zone of the original pyrochlore lattice. (b) Under the $\boldsymbol{Q} = 2\pi(001)$ Melko-Hertog-Gingras (MHG) spin ice state, the unit cell is enlarged. The plot is the magnetic Brillouin zone corresponding to the enlarged unit cell. (c) The spin configuration of the MHG spin ice state. It is a 2-in–2-out spin ice state with $\boldsymbol{Q} = 2\pi(001)$ ordering wave vector. The magnetic unit cell with $\tilde{\boldsymbol{b}}_i$'s is defined in Appendix A. (d) The folded band of the Ir electrons without $f$-$d$ exchange develops a quadratic touching at $\tilde{\Gamma}$. High symmetry momentum lines are defined in (b) as blue lines.

the band-structure properties from the symmetry point of view. For our choice of the propagating wave vector, the MHG spin ice state breaks the lattice translations, $t_1$ and $t_2$. Here, $t_1$ and $t_2$ translate the system by the lattice basis vector $\boldsymbol{b}_1 \equiv (0, 1/2, 1/2)$ and $\boldsymbol{b}_2 \equiv (1/2, 0, 1/2)$, respectively. It turns out that, the combination of time reversal and $t_1$ or $t_2$, i.e.,

$$\tilde{\mathcal{T}}_1 \equiv t_1 \circ \mathcal{T}, \qquad \tilde{\mathcal{T}}_2 \equiv t_2 \circ \mathcal{T}, \tag{14}$$

remains to be a symmetry of the system after the development of the Pr magnetic order. These two symmetries of the MHG spin state are analogous to the staggered time reversal of the antiferromagnetic Néel state for a square lattice Heisenberg model. Like the pure time reversal, $\tilde{\mathcal{T}}_1$ and $\tilde{\mathcal{T}}_2$ are antiunitary operations. Similar antiunitary symmetry has been considered in the early proposal of antiferromagnetc topological insulator by Mong, Essin, and Moore [61]. Because of the involvement of the lattice translations, $\tilde{\mathcal{T}}_1$ and $\tilde{\mathcal{T}}_2$ do not lead to the Kramers degeneracy for all the time reversal invariant momenta in the magnetic Brillouin zone. It is ready to confirm that

$$\tilde{\mathcal{T}}_1|\tilde{\Gamma}, \uparrow\rangle = i|\tilde{\Gamma}, \downarrow\rangle, \qquad \tilde{\mathcal{T}}_2|\tilde{\Gamma}, \uparrow\rangle = i|\tilde{\Gamma}, \downarrow\rangle, \tag{15}$$

$$\tilde{\mathcal{T}}_1|\tilde{M}, \uparrow\rangle = i|\tilde{M}, \downarrow\rangle, \qquad \tilde{\mathcal{T}}_2|\tilde{M}\uparrow\rangle = -i|\tilde{M}, \downarrow\rangle, \tag{16}$$

$$\tilde{\mathcal{T}}_1|\tilde{R}, \uparrow\rangle = -i|\tilde{R}, \downarrow\rangle, \qquad \tilde{\mathcal{T}}_2|\tilde{R}, \uparrow\rangle = -i|\tilde{R}, \downarrow\rangle, \tag{17}$$

and $\tilde{\mathcal{T}}_1^2 = \tilde{\mathcal{T}}_2^2 = -1$ for the momentum points at $\tilde{\Gamma}$, $\tilde{M}$, and $\tilde{R}$; and $\tilde{\mathcal{T}}_1^2 = \tilde{\mathcal{T}}_2^2 = +1$ for the momentum points at $\tilde{X}$, $\tilde{Z}$, and $\tilde{A}$. Note that $\tilde{\Gamma}$, $\tilde{M}$, and $\tilde{R}$ are also time-reversal invariant momenta of the crystal Brillouin zone while $\tilde{X}$, $\tilde{Z}$, and $\tilde{A}$ are not. It immediately indicates that there are twofold Kramers degeneracy at the $\tilde{\Gamma}$, $\tilde{M}$, and $\tilde{R}$ points, but not for the $\tilde{X}$, $\tilde{Z}$, and $\tilde{A}$ points. Actually, the former holds for other time-reversal invariant momenta of the crystal Brillouin zone. To confirm the above prediction, we carry out the explicit calculation of the Ir band structure in the presence of the Pr Ising magnetic order. As we show in Fig. 3 for four specific choices of the $f$-$d$ exchange couplings, there exist emergent twofold Kramers degeneracies with Dirac-band touchings at the $\tilde{\Gamma}$, $\tilde{M}$, and $\tilde{R}$ points.

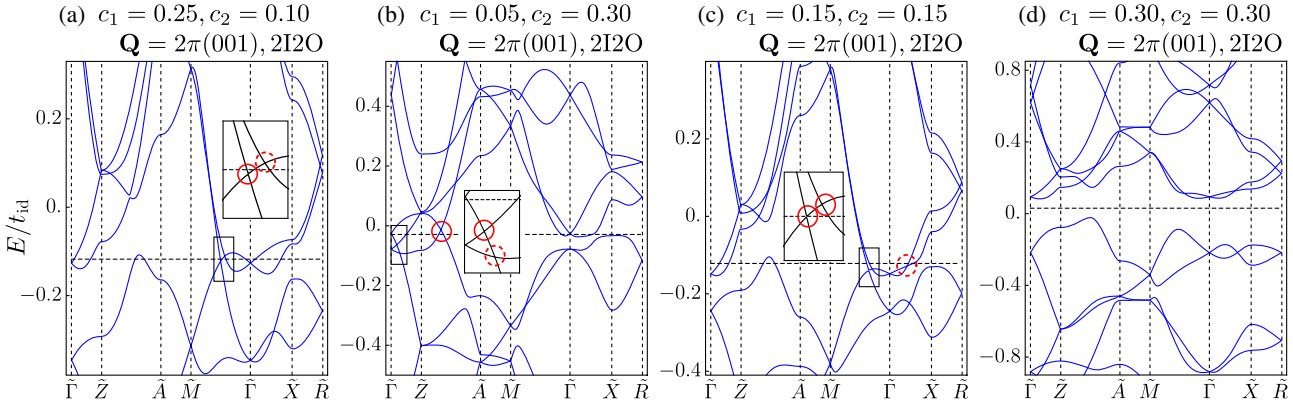


FIG. 3. Evolution of the Ir band structure as a function of $f$-$d$ exchange parameters $c_1$ and $c_2$. The dashed (solid) circle marks the usual (double) Weyl node. Here, the usual Weyl node has linear dispersions along all three momentum directions, while the double Weyl node has quadratic dispersions along two momentum directions and linear along one momentum direction [62]. For sufficiently large parameters in (d), the Weyl nodes disappear and a band gap is opened. Here, "2I2O" refers to the 2-in–2-out spin configuration. The energy unit in the plots is $t_{\rm id}$. The dashed line refers to the Fermi energy. Here, only a finite energy range is plotted for clarity. See Appendix B for the full band structures.

### B. Magnetic Weyl nodes

Besides the emergent and symmetry-protected Dirac-band touchings at the $\tilde{\Gamma}$, $\tilde{M}$, and $\tilde{R}$ points, we discover the presence of the Weyl nodes in the reconstructed Ir band structure in Fig. 3. The reconstructed Ir band structure is determined by the $f$-$d$ exchange couplings. The actual couplings of the $f$-$d$ exchange in the material $Pr_2Ir_2O_7$ are unknown to us. To proceed, we fix the tight-binding part of the Ir hopping Hamiltonian and study the band-structure phase diagram of Ir electrons by varying the $f$-$d$ exchange couplings. This approach is not designed to be self-consistent, but is phenomenological. The Pr Ising order, that is observed experimentally [36], is used as the input information to the Ir band-structure calculation in this section. We expect the realistic case for $Pr_2Ir_2O_7$ would be located at one specific parameter point in the phase diagram. It is possible that the pressure could vary the exchange couplings and allow the system to access different parameters of the phase diagram.

In Fig. 4, we depict our phase diagram according to the exchange couplings. For small exchange couplings, a semimetal is always obtained. The name "semimetal" here not only refers to the Dirac-band touching or dispersion at some time-reversal invariant momenta, but also refers to the (topologically protected) Weyl nodes in the magnetic Brillouin zone. In fact, Weyl semimetal with the surface Fermi arcs was first predicted for pyrochlore iridates with the all-in all-out magnetic order, and the magnetic order is suggested to be driven by the Ir electron correlation [15]. In our result here, the magnetic order comes from the Pr Ising order, and the time-reversal symmetry breaking is then transmitted to the Ir conduction electron via the $f$-$d$ exchange. The Pr Ising magnetic order is not the simple all-in all-out magnetic order. It was also suggested that the correlation-driven Weyl semimetal for pyrochlore iridates appears in a rather narrow parameter regime [16]. The $f$-$d$ exchange, however, could significantly enlarge the parameter regime for Weyl semimetal [14]. Indeed, in Fig. 4, the semimetal region does support several Weyl nodes near the Fermi level, and thus, we expect the usual properties for Weyl semimetal [15] to hold in this regime. Moreover, since the $f$-$d$ exchange coupling is much smaller than the effective hoppings of the Ir electrons, so the realistic case for the ordered $Pr_2Ir_2O_7$ is expected to occur in the semimetallic region of Fig. 4.

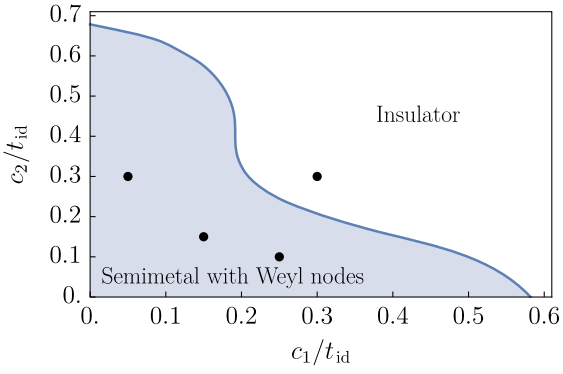


FIG. 4. Phase diagram for the Ir band structure in the parameter space of the $f$-$d$ exchange couplings. The bold dots refer to the four parameter choices in Fig. 3.

## IV. ROLE OF EXTERNAL MAGNETIC FIELDS

To further control the physical property of the system, we suggest to apply an (uniform) external magnetic field to the system. As we have explained in Sec. I, the magnetic field would primarily couple to the Pr local moments. A uniform magnetic field induces a finite magnetic polarization on the Pr local moments, and thus breaks the $\tilde{\mathcal{T}}_1$ and $\tilde{\mathcal{T}}_2$ symmetries of the ordered $Pr_2Ir_2O_7$. As a consequence, the emergent Dirac-band touchings at the $\tilde{\Gamma}$, $\tilde{M}$, and $\tilde{R}$ points, that are protected by the $\tilde{\mathcal{T}}_1$ and $\tilde{\mathcal{T}}_2$ symmetries, should disappear immediately in a generic magnetic field along a random direction. Here, the choice of a random direction for the magnetic field simply avoids the accidental degeneracy and band touching that is protected by the reduced lattice symmetry of the system if the field is applied along high symmetry directions.

Like the previous section where the Ir band structure is controlled by the $f$-$d$ exchange and the Ir tight-binding model, the Ir band structure in the magnetic field requires the knowledge of the Pr magnetic state that is now modified by the external magnetic field. As we have explained in Sec. I, the external magnetic field first modifies the Pr magnetic state and then indirectly influences the Ir band structure through the $f$-$d$ exchange interaction. For the Pr subsystem, we consider the following Hamiltonian,

$$H_{\mathrm{Pr}} = \tilde{H}_{\mathrm{ex}} + H_{\mathrm{Zeeman}}, \tag{18}$$

where the exchange part includes both the first-neighbor and third-neighbor Ising exchange interactions. Since here the Pr local moment is set to be an Ising d.o.f., the magnetic phase diagram of the Pr moments is readily obtained by comparing energies of candidate ground states. The magnetic phase diagram for the Pr moments is depicted in Fig. 5, where three different directions of magnetic fields are considered.

Here, we focus on one specific field orientation, $\hat{n} \equiv (1,1,1)/\sqrt{3}$, and evaluate the feedback of the Pr magnetic state on the Ir conduction electrons. Besides the original MHG spin ice state, two additional spin states are obtained. While the Ir band structure in the presence of the MHG spin state stays the same as the ones in Sec. III under this approximation, this should be the caveat of the approximation of the Pr local moment as the Ising spin that ignores the quantum nature of the Pr local moment. In reality, the magnetic field would create a finite polarization for the Pr local moment and modifies the Ir band structure

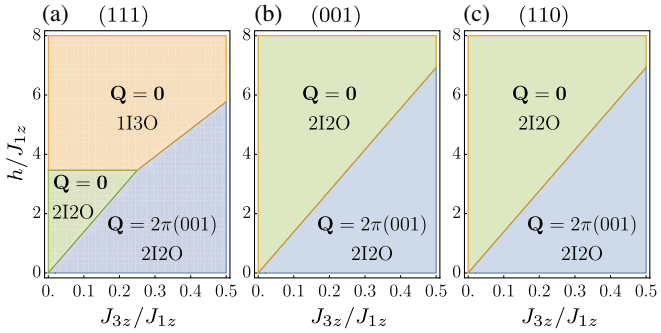


FIG. 5. Phase diagram of the Pr local moments under the external magnetic fields along different directions. Here, "1I3O" refers to "1-in–3-out" spin configuration.

immediately, even though the modification can be small. This would allow us to move the positions of the Weyl nodes in the momentum space. The other two spin configurations of the Pr moments, that result from strong magnetic field, have an ordering wave vector $\boldsymbol{Q} = \mathbf{0}$ and restore the lattice translation symmetry. Hence, we expect two different Ir band structures for the $\boldsymbol{Q} = \mathbf{0}$ 2-in–2-out and 1-in–3-out Pr spin states. In Fig. 6, we depict the Ir band structures for specific choices of the $f$-$d$ exchanges with two $\boldsymbol{Q} = \mathbf{0}$ spin configurations from the phase diagram in Fig. 5(a). By letting the Pr moments have the specified spin configurations, we explicitly calculate the Ir band structure that is depicted in Fig. 6. We find that the Dirac-band touchings at the $\tilde{\Gamma}(\equiv\Gamma)$, $\tilde{R}(\equiv L)$ points are absent in the magnetic field, and now the magnetic unit cell is identical to the crystal unit cell. Moreover, although the time-reversal symmetry breaking is transmitted by the Pr spin configuration due to the external magnetic field, the overall effect is equivalent to applying the time-reversal symmetry breaking to the Ir Luttinger semimetal. Since Luttinger semimetal can be regarded as the parent state of the Weyl semimetal [19,42], it seems natural to expect the occurrence of the Weyl nodes. Indeed, as we show in Fig. 7, we obtain the Weyl semimetal (or Weyl metal) for a large parameter regime in the phase diagram.

With large magnetic fields along (001) and (110) directions, the $\boldsymbol{Q} = \mathbf{0}$ state is obtained for the Pr local moments under this approximation [see Figs. 5(b) and 5(c)]. This Pr spin state is the same as one of the spin states when the field

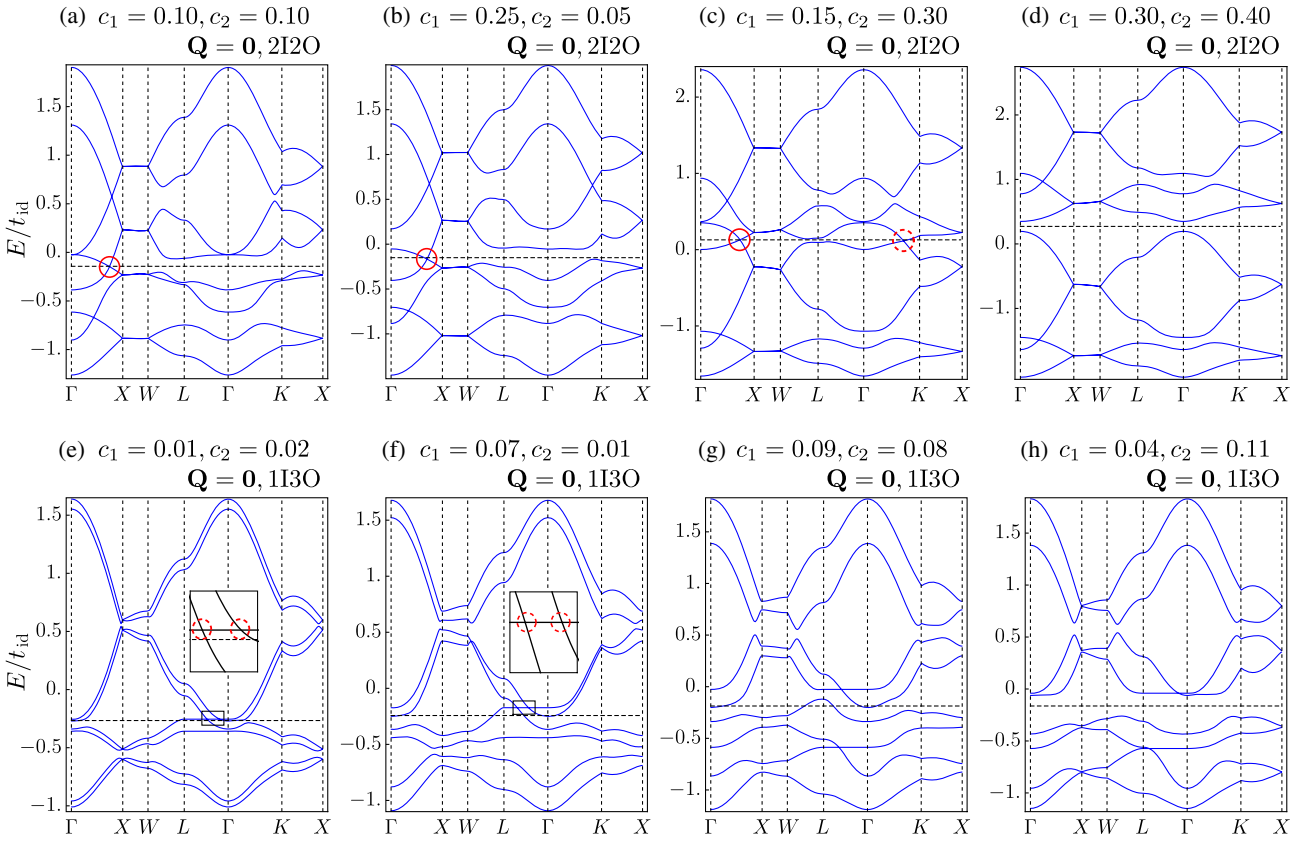


FIG. 6. Evolution of the Ir band structure as a function of $f$-$d$ exchange parameters for (a)–(d) 1-in–3-out (1I3O) and (e)–(h) 2-in–2-out (2I2O) Pr magnetic states with $\boldsymbol{Q} = 0$ from Fig. 5(a). The dashed (solid) circle marks the usual (double) Weyl node. In (a) and (b), one band from $L$ to $\Gamma$ is flat. This is accidental for the nearest-neighbor hopping model and is dispersive if further neighbor hoppings are included [16]. In (g), the Weyl nodes are actually at different energies. The energy unit in the plots is $t_{\mathrm{id}}$. The dashed line refers to the Fermi energy.

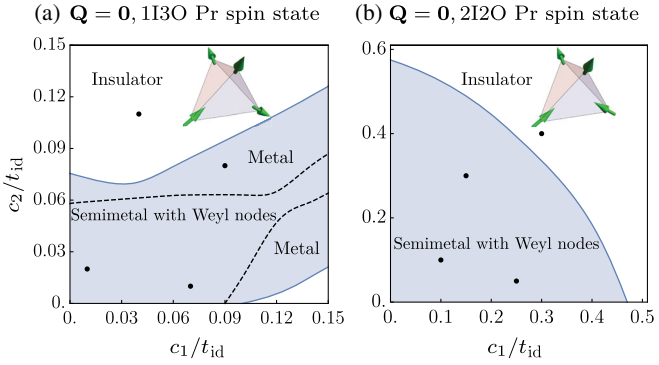


FIG. 7. Phase diagram for the Ir band structure in the parameter space of the $f$-$d$ exchange couplings for different Pr magnetic states from Fig. 5(a). The bold dots in the plots are the parameter choices for Fig. 6.

is applied along the (111) direction, and there it does not bring different Ir band structures under this approximation.

## V. DISCUSSION

Here, we first summarize our understanding of the rich physics in $Pr_2Ir_2O_7$ and suggest future experiments to further reveal its physics, and then provide a general discussion and vision for hybrid quantum materials of the similar kind. In the previous field theoretical work by one of the authors, we pointed out that the Pr subsystem of $Pr_2Ir_2O_7$ is proximate to a quantum phase transition from the $U(1)$ quantum spin liquid to the Ising magnetic order [41]. The proximate Ising magnetic order, that is obtained from the condensation of the magnetic monopoles in the $U(1)$ quantum spin liquid, breaks the lattice translation and is precisely the one that is observed in the neutron scattering experiments [36]. This theoretical work indicates that the paramagnetic state of disordered $Pr_2Ir_2O_7$ sample is likely to be a $U(1)$ quantum spin liquid. In the current work, we focus on the magnetically ordered $Pr_2Ir_2O_7$ sample. We have developed a systematic modeling to understand the interplay between the Ir conduction electrons and the Pr local moments for $Pr_2Ir_2O_7$. Our theory and general thought can be well extended to other hybrid quantum materials with both local moments and conduction electrons. We use the existing experimental results, such as the Luttinger semimetal of the Ir conduction electrons and the MHG spin ice state of the Pr local moments, as the basic input information for our theoretical framework, and study the band reconstruction of the Ir conduction electrons in the presence of the Pr Ising magnetic order. We predict that the symmetry-protected Dirac-band touchings emerge at the time-reversal invariant momenta and the symmetry protection comes from the magnetic translation symmetry of the MHG spin ice state for the Pr subsystem. Moreover, there generically exist Weyl nodes of different kinds both in the ordered $Pr_2Ir_2O_7$ samples and $Pr_2Ir_2O_7$ in the external magnetic fields.

Based on our prediction about the nontrivial Ir band structure after the reconstruction from the Pr Ising magnetic state, we here propose the future experiments. The quadratic band touching at the $\Gamma$ point of the nonmagnetic $Pr_2Ir_2O_7$ sample was first revealed by the angle-resolved photoemission spectroscopy (ARPES) [42]. Thus, the reconstructed Ir band structure in the magnetically ordered $Pr_2Ir_2O_7$ sample (without the magnetic field) would be best detected by the ARPES. Although the Pr magnetic domain may complicate the data analysis, the nontrivial features at and near the $\Gamma$ point should not be modified by the multiple Pr magnetic domains as these features are near zero momentum properties. On the other hand, the optical measurements are useful for detecting the interband particle-hole transition near the band touching points that gives rise to power-law optical conductivity. As ARPES fails in the presence of magnetic fields, the optical measurements can thus be complementary. The Dirac-band touchings at some of the time reversal invariant momenta, that are protected by the magnetic translation of the MHG spin ice state, would immediately disappear when the magnetic field is applied. This prediction could be a sharp feature for the experimental confirmation in the optical measurement.

Besides the direct band-structure measurements with ARPES and/or optics, the magnetotransport can serve as a useful indirect probe. Because of the breaking of the cubic symmetry, the Weyl semimetal that is induced by the external magnetic field would show anomalous Hall effects. Furthermore, we point out the field-driven metal-insulator transition. Although it was not emphasized in Sec. IV, the large portion of the semimetallic region in the phase diagram of Fig. 4 is converted into the insulating region in the phase diagram of Fig. 7(a). From the experience in $Nd_2Ir_2O_7$ with the dipole-octupole $Nd^{3+}$ magnetic ions [14,32,63,64], this field-driven metal-insulator transition via the $f$-$d$ exchange could be the most visible experimental signature in the transport measurement and may find an application in magnetic storage and magnetic control of electric transports. Finally, as we have mentioned in Sec. II A, we note several theoretical works have considered the effect of the long-range Coulomb interaction on the Ir conduction electron with the quadratic band touching [17,50–56]. Because of the partial screening of the Coulomb interaction, various interesting correlated phases may be stabilized. Now we have included the Pr magnetism into the system; it can thus be interesting to consider the long-range Coulomb interaction on top of the reconstructed Ir bands in the presence of the Pr magnetism in the future work.

We explain the feasibility of the magnetic control of the physical properties such as magnetic, transport and band-structure properties of $Pr_2Ir_2O_7$. From the experience with the rare-earth pyrochlores and the rare-earth triangular magnets, the interactions between the rare-earth local moments are usually quite small [38,64–69]. In $Pr_2Ir_2O_7$, the Ir conduction electrons mediate the RKKY interaction

between the Pr local moments and could slightly enhance the energy scale of the Pr-Pr interactions. Even that, the Pr-Pr energy scale is of the order of ∼10 K from the early susceptibility measurement [34]. Because of the low-energy scale of Pr-Pr interactions, a magnetic field of the order of several Tesla could readily modify the Pr magnetic structures. Indeed, early transport measurement in magnetic fields have already hinted the change of the Pr magnetic structures [34]. Although the external field that one actually applies can be small, the indirect effect on the Ir conduction electron is huge due to the large internal field that is generated by the $f$-$d$ exchange. *This amplification effect* is rather nontrivial and arises from the separation of energy scales in $Pr_2Ir_2O_7$. This effect can be immediately tested in the current laboratory setting.

From a much broader perspective, $Pr_2Ir_2O_7$ is a prototype and singular example of hybrid quantum materials with both itinerant electrons and local moments. The separation of the energy scales among distinct d.o.f. allows the quantum control between each other. Quite recently, several rare-earth-based hybrid quantum materials have been discovered and studied. The candidate examples are the half-Heusler compounds $RGeX$ ($R$ = rare earth, $X$ = Si/Ge) [70] and the rare-earth pnictide CeSb where the itinerant electron part was proposed to realize Weyl semimetals [71,72]. The rare-earth parts of these materials could then contribute to magnetism. In the half-Heusler compounds $RGeX$, the interesting singular angular magnetoresistance was observed and is believed to arise from the coupling between the rare-earth moments and the itinerant electrons. Because of the similarity of the physical contents in these systems with $Pr_2Ir_2O_7$, we propose similar physics and theories could be well realized and readily extended to these new materials. Therefore, we think our work could inspire further interest in these hybrid quantum materials with both itinerant electrons and local moments.

## ACKNOWLEDGMENTS

We thank C. Broholm for the early discussion about the Pr magnetic order of $Pr_2Ir_2O_7$ at the University of Cambridge, a correspondence with S. Nakatsuji, useful conversation with Roger Mong, Zhong Wang, and Yi Zhou, and an early collaboration with Michael Hermele from CU Boulder. This work is supported by the Ministry of Science and Technology of China with Grant No. 2016YFA0301001, the start-up fund, and the First-Class University construction fund of Fudan University, and the Thousand-Youth-Talent program of China.

## APPENDIX A: SUBLATTICES AND CRYSTAL MOMENTA FOR $Pr_2Ir_2O_7$

In $Pr_2Ir_2O_7$, both Ir and Pr pyrochlore lattices are composed of linked tetrahedra and can be viewed as FCC lattice with primitive lattice vectors

$$\boldsymbol{b}_1 = \left(0, \frac{1}{2}, \frac{1}{2}\right), \tag{A1}$$

$$\boldsymbol{b}_2 = \left(\frac{1}{2}, 0, \frac{1}{2}\right), \tag{A2}$$

$$\boldsymbol{b}_3 = \left(\frac{1}{2}, \frac{1}{2}, 0\right). \tag{A3}$$

After choosing one of the Ir site as a reference point, the reference positions of four Ir sublattices can be set to be

$$\mathrm{Ir}_1 = (0,0,0), \qquad \mathrm{Ir}_2 = \left(0, \frac{1}{4}, \frac{1}{4}\right), \tag{A4}$$

$$\mathrm{Ir}_3 = \left(\frac{1}{4}, 0, \frac{1}{4}\right), \qquad \mathrm{Ir}_4 = \left(\frac{1}{4}, \frac{1}{4}, 0\right). \tag{A5}$$

Likewise, for the Pr subsystem we have the reference positions of four Pr sublattices as

$$\mathrm{Pr}_1 = \left(0, \frac{1}{2}, 0\right), \qquad \mathrm{Pr}_2 = \left(0, \frac{3}{4}, \frac{1}{4}\right), \tag{A6}$$

$$\mathrm{Pr}_3 = \left(\frac{1}{4}, \frac{1}{2}, \frac{1}{4}\right), \qquad \mathrm{Pr}_4 = \left(\frac{1}{4}, \frac{3}{4}, 0\right). \tag{A7}$$

The crystal momenta in Fig. 2 are

$$\tilde{\Gamma} = (0,0,0), \quad \tilde{M} = (2\pi, 0, 0), \quad \tilde{R} = (\pi, \pi, \pi), \tag{A8}$$

$$\tilde{X} = (\pi, \pi, 0), \quad \tilde{Z} = (0, 0, \pi), \quad \tilde{A} = (2\pi, 0, \pi). \tag{A9}$$

In Melko-Hertog-Gingras spin ice state, the magnetic unit cell of $Pr_2Ir_2O_7$ is twice the crystal unit cell with new lattice vectors

$$\tilde{\boldsymbol{b}}_1 = (0,0,1), \tag{A10}$$

$$\tilde{\boldsymbol{b}}_2 = \left(\frac{1}{2}, -\frac{1}{2}, 0\right), \tag{A11}$$

$$\tilde{\boldsymbol{b}}_3 = \left(\frac{1}{2}, \frac{1}{2}, 0\right). \tag{A12}$$

## APPENDIX B: THE COMPLETE Ir BAND STRUCTURES IN MELKO-HERTOG-GINGRAS SPIN ICE STATE

In Fig. 3 of the main text we have set a limited energy window to show the details of reconstructed Ir band structure near Fermi the surface where different types of the Weyl node appear. Here, we show the complete Ir band structures in Fig. 8.

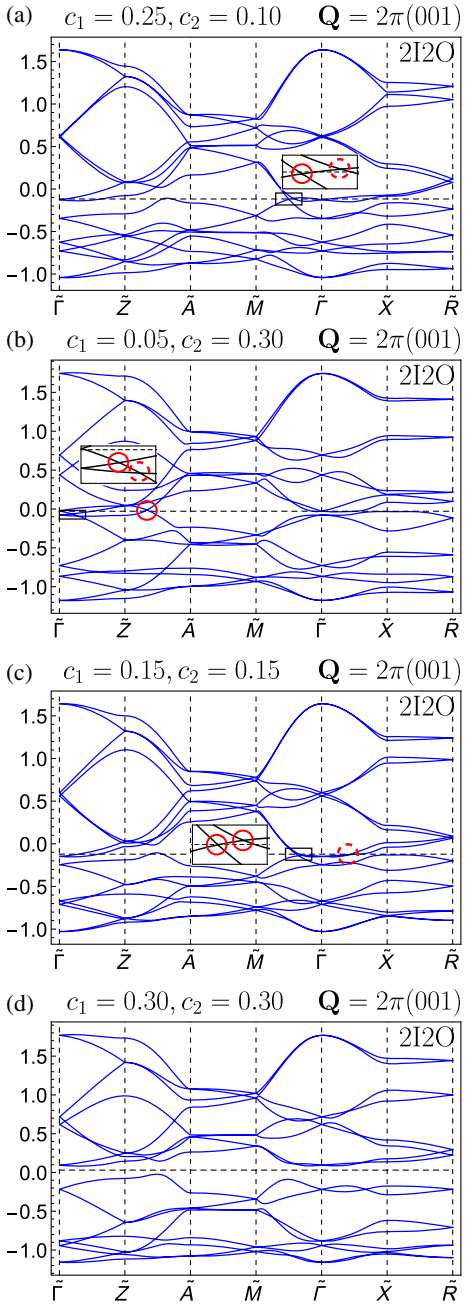


FIG. 8. The complete Ir band structure and its evolution as a function of $f$-$d$ exchange $c_1$ and $c_2$. The dashed (solid) circle marks the usual (double) Weyl node where the definition of different types of Weyl node has given in main text. A sufficient strong $f$-$d$ exchange coupling wipes out Weyl nodes near the Fermi surface and opens band gaps. The energy unit is $t_{\mathrm{id}}$. The dashed line refers to the Fermi energy.


[1] M. Z. Hasan and C. L. Kane, *Colloquium: Topological Insulators*, Rev. Mod. Phys. **82**, 3045 (2010).

[2] X.-L. Qi and S.-C. Zhang, *Topological Insulators and Superconductors*, Rev. Mod. Phys. **83**, 1057 (2011).

[3] N. P. Armitage, E. J. Mele, and A. Vishwanath, *Weyl and Dirac Semimetals in Three Dimensional Solids*, Rev. Mod. Phys. **90**, 015001 (2018).

[4] Y. Ando and L. Fu, *Topological Crystalline Insulators and Topological Superconductors: From Concepts to Materials*, Annu. Rev. Condens. Matter Phys. **6**, 361 (2015).

[5] R. Yu, W. Zhang, H.-J. Zhang, S.-C. Zhang, X. Dai, and Z. Fang, *Quantized Anomalous Hall Effect in Magnetic Topological Insulators*, Science **329**, 61 (2010).

[6] C.-Z. Chang, J. Zhang, X. Feng, J. Shen, Z. Zhang, M. Guo, K. Li, Y. Ou, P. Wei, L.-L. Wang, Z.-Q. Ji, Y. Feng, S. Ji, X. Chen, J. Jia, X. Dai, Z. Fang, S.-C. Zhang, K. He, Y. Wang *et al.*, *Experimental Observation of the Quantum Anomalous Hall Effect in a Magnetic Topological Insulator*, Science **340**, 167 (2013).

[7] C.-X. Liu, S.-C. Zhang, and X.-L. Qi, *The Quantum Anomalous Hall Effect: Theory and Experiment*, Annu. Rev. Condens. Matter Phys. **7**, 301 (2016).

[8] D. Pesin and L. Balents, *Mott Physics and Band Topology in Materials with Strong Spinorbit Interaction*, Nat. Phys. **6**, 376 (2010).

[9] D. Yanagishima and Y. Maeno, *Metal-Nonmetal Changeover in Pyrochlore Iridates*, J. Phys. Soc. Jpn. **70**, 2880 (2001).

[10] K. Matsuhira, M. Wakeshima, Y. Hinatsu, and S. Takagi, *MetalInsulator Transitions in Pyrochlore Oxides* $Ln_2Ir_2O_7$, J. Phys. Soc. Jpn. **80**, 094701 (2011).

[11] B.-J. Yang and Y. B. Kim, *Topological Insulators and Metal-Insulator Transition in the Pyrochlore Iridates*, Phys. Rev. B **82**, 085111 (2010).

[12] W. Witczak-Krempa, T. P. Choy, and Y. B. Kim, *Gauge Field Fluctuations in Three-Dimensional Topological Mott Insulators*, Phys. Rev. B **82**, 165122 (2010).

[13] A. Go, W. Witczak-Krempa, G. S. Jeon, K. Park, and Y. B. Kim, *Correlation Effects on 3D Topological Phases: From Bulk to Boundary*, Phys. Rev. Lett. **109**, 066401 (2012).

[14] G. Chen and M. Hermele, *Magnetic Orders and Topological Phases from $f$-$d$ Exchange in Pyrochlore Iridates*, Phys. Rev. B **86**, 235129 (2012).

[15] X. Wan, A. M. Turner, A. Vishwanath, and S. Y. Savrasov, *Topological Semimetal and Fermi-Arc Surface States in the Electronic Structure of Pyrochlore Iridates*, Phys. Rev. B **83**, 205101 (2011).

[16] W. Witczak-Krempa and Y. B. Kim, *Topological and Magnetic Phases of Interacting Electrons in the Pyrochlore Iridates*, Phys. Rev. B **85**, 045124 (2012).

[17] E.-G. Moon, C. Xu, Y. B. Kim, and L. Balents, *Non-Fermi-Liquid and Topological States with Strong Spin-Orbit Coupling*, Phys. Rev. Lett. **111**, 206401 (2013).

[18] S. B. Lee, A. Paramekanti, and Y. B. Kim, *RKKY Interactions and the Anomalous Hall Effect in Metallic Rare-Earth Pyrochlores*, Phys. Rev. Lett. **111**, 196601 (2013).

[19] L. Savary, E.-G. Moon, and L. Balents, *New Type of Quantum Criticality in the Pyrochlore Iridates*, Phys. Rev. X **4**, 041027 (2014).

[20] W. Witczak-Krempa, G. Chen, Y. B. Kim, and L. Balents, *Correlated Quantum Phenomena in the Strong Spin-Orbit Regime*, Annu. Rev. Condens. Matter Phys. **5**, 57 (2014).

[21] R. Wang, A. Go, and A. J. Millis, *Electron Interactions, Spin-Orbit Coupling, and Intersite Correlations in Pyrochlore Iridates*, Phys. Rev. B **95**, 045133 (2017).

[22] F. Lambert, A. P. Schnyder, R. Moessner, and I. Eremin, *Quasiparticle Interference from Different Impurities on the Surface of Pyrochlore Iridates: Signatures of the Weyl Phase*, Phys. Rev. B **94**, 165146 (2016).
[23] F. F. Tafti, J. J. Ishikawa, A. McCollam, S. Nakatsuji, and S. R. Julian, *Pressure-Tuned Insulator to Metal Transition in* $Eu_2Ir_2O_7$, Phys. Rev. B **85**, 205104 (2012).
[24] J. J. Ishikawa, E. C. T. O'Farrell, and S. Nakatsuji, *Continuous Transition between Antiferromagnetic Insulator and Paramagnetic Metal in the Pyrochlore Iridate* $Eu_2Ir_2O_7$, Phys. Rev. B **85**, 245109 (2012).
[25] S. Zhao, J. M. Mackie, D. E. MacLaughlin, O. O. Bernal, J. J. Ishikawa, Y. Ohta, and S. Nakatsuji, *Magnetic Transition, Long-Range Order, and Moment Fluctuations in the Pyrochlore Iridate* $Eu_2Ir_2O_7$, Phys. Rev. B **83**, 180402 (2011).
[26] S. M. Disseler, C. Dhital, A. Amato, S. R. Giblin, C. de la Cruz, S. D. Wilson, and M. J. Graf, *Magnetic Order in the Pyrochlore Iridates* $A_2Ir_2O_7$ *(A =* Y, *Yb)*, Phys. Rev. B **86**, 014428 (2012).
[27] S. M. Disseler, C. Dhital, T. C. Hogan, A. Amato, S. R. Giblin, C. de la Cruz, A. Daoud-Aladine, S. D. Wilson, and M. J. Graf, *Magnetic Order and the Electronic Ground State in the Pyrochlore Iridate* $Nd_2Ir_2O_7$, Phys. Rev. B **85**, 174441 (2012).
[28] W. K. Zhu, M. Wang, B. Seradjeh, F. Yang, and S. X. Zhang, *Enhanced Weak Ferromagnetism and Conductivity in Hole-Doped Pyrochlore Iridate* $Y_2Ir_2O_7$, Phys. Rev. B **90**, 054419 (2014).
[29] H. Takatsu, K. Watanabe, K. Goto, and H. Kadowaki, *Comparative Study of Low-Temperature X-Ray Diffraction Experiments on* $R_2Ir_2O_7$ *(R =* Nd, Eu, andPr*)*, Phys. Rev. B **90**, 235110 (2014).
[30] G. Prando, R. Dally, W. Schottenhamel, Z. Guguchia, S.-H. Baek, R. Aeschlimann, A. U. B. Wolter, S. D. Wilson, B. Büchner, and M. J. Graf, *Influence of Hydrostatic Pressure on the Bulk Magnetic Properties of* $Eu_2Ir_2O_7$, Phys. Rev. B **93**, 104422 (2016).
[31] R. Flint and T. Senthil, *Chiral RKKY Interaction in* $Pr_2Ir_2O_7$, Phys. Rev. B **87**, 125147 (2013).
[32] Z. Tian, Y. Kohama, T. Tomita, H. Ishizuka, T. H. Hsieh, J. J. Ishikawa, K. Kindo, L. Balents, and S. Nakatsuji, *Field-Induced Quantum Metalinsulator Transition in the Pyrochlore Iridate* $Nd_2Ir_2O_7$, Nat. Phys. **12**, 134 (2016).
[33] Y. Machida, S. Nakatsuji, S. Onoda, T. Tayama, and T. Sakakibara, *Time-Reversal Symmetry Breaking and Spontaneous Hall Effect without Magnetic Dipole Order*, Nature (London) **463**, 210 (2010).
[34] S. Nakatsuji, Y. Machida, Y. Maeno, T. Tayama, T. Sakakibara, J. van Duijn, L. Balicas, J. N. Millican, R. T. Macaluso, and J. Y. Chan, *Metallic Spin-Liquid Behavior of the Geometrically Frustrated Kondo Lattice* $Pr_2Ir_2O_7$, Phys. Rev. Lett. **96**, 087204 (2006).
[35] Y. Tokiwa, J. J. Ishikawa, S. Nakatsuji, and P. Gegenwart, *Quantum Criticality in a Metallic Spin Liquid*, Nat. Mater. **13**, 356 (2014).
[36] D. E. MacLaughlin, O. O. Bernal, L. Shu, J. Ishikawa, Y. Matsumoto, J.-J. Wen, M. Mourigal, C. Stock, G. Ehlers, C. L. Broholm, Y. Machida, K. Kimura, S. Nakatsuji, Y. Shimura, and T. Sakakibara, *Unstable Spin-Ice Order in the Stuffed Metallic Pyrochlore* $Pr_{2+x}Ir_{2-x}O_{7-\delta}$, Phys. Rev. B **92**, 054432 (2015).
[37] R. G. Melko, B. C. den Hertog, and M. J. P. Gingras, *Long-Range Order at Low Temperatures in Dipolar Spin Ice*, Phys. Rev. Lett. **87**, 067203 (2001).
[38] K. A. Ross, L. Savary, B. D. Gaulin, and L. Balents, *Quantum Excitations in Quantum Spin Ice*, Phys. Rev. X **1**, 021002 (2011).
[39] J. S. Gardner, S. R. Dunsiger, B. D. Gaulin, M. J. P. Gingras, J. E. Greedan, R. F. Kiefl, M. D. Lumsden, W. A. MacFarlane, N. P. Raju, J. E. Sonier, I. Swainson, and Z. Tun, *Cooperative Paramagnetism in the Geometrically Frustrated Pyrochlore Antiferromagnet* $Tb_2Ti_2O_7$, Phys. Rev. Lett. **82**, 1012 (1999).
[40] L. D. Pan, N. J. Laurita, K. A. Ross, B. D. Gaulin, and N. P. Armitage, *A Measure of Monopole Inertia in the Quantum Spin Ice* $Yb_2Ti_2O_7$, Nat. Phys. **12**, 361 (2016).
[41] G. Chen, *"Magnetic Monopole", Condensation of the Pyrochlore Ice* $U(1)$ *Quantum Spin Liquid: Application to* $Pr_2Ir_2O_7$ *and* $Yb_2Ti_2O_7$, Phys. Rev. B **94**, 205107 (2016).
[42] T. Kondo, M. Nakayama, R. Chen, J. J. Ishikawa, E.-G. Moon, T. Yamamoto, Y. Ota, W. Malaeb, H. Kanai, Y. Nakashima, Y. Ishida, R. Yoshida, H. Yamamoto, M. Matsunami, S. Kimura, N. Inami, K. Ono, H. Kumigashira, S. Nakatsuji, L. Balents *et al.*, *Quadratic Fermi Node in a 3D Strongly Correlated Semimetal*, Nat. Commun. **6**, 10042 (2015).
[43] F. Ishii, Y. P. Mizuta, T. Kato, T. Ozaki, H. Weng, and S. Onoda, *First-Principles Study on Cubic Pyrochlore Iridates* $Y_2Ir_2O_7$ *and* $Pr_2Ir_2O_7$, J. Phys. Soc. Jpn. **84**, 073703 (2015).
[44] B. Cheng, T. Ohtsuki, D. Chaudhuri, M. Lippmaa, and N. P. Armitage, *Dielectric Anomalies and Interactions in the Three-Dimensional Quadratic Band Touching Luttinger Semimetal* $Pr_2Ir_2O_7$, Nat. Commun. **8**, 2097 (2017).
[45] B. A. Bernevig, T. L. Hughes, and S.-C. Zhang, *Quantum Spin Hall Effect and Topological Phase Transition in HgTe Quantum Wells*, Science **314**, 1757 (2006).
[46] C. Brüne, C. X. Liu, E. G. Novik, E. M. Hankiewicz, H. Buhmann, Y. L. Chen, X. L. Qi, Z. X. Shen, S. C. Zhang, and L. W. Molenkamp, *Quantum Hall Effect from the Topological Surface States of Strained Bulk HgTe*, Phys. Rev. Lett. **106**, 126803 (2011).
[47] B. J. Kim, H. Jin, S. J. Moon, J.-Y. Kim, B.-G. Park, C. S. Leem, J. Yu, T. W. Noh, C. Kim, S.-J. Oh, J.-H. Park, V. Durairaj, G. Cao, and E. Rotenberg, *Novel* $J_{\rm eff} = 1/2$ *Mott State Induced by Relativistic Spin-Orbit Coupling in* $Sr_2IrO_4$, Phys. Rev. Lett. **101**, 076402 (2008).
[48] G. Chen and L. Balents, *Spin-Orbit Effects in* $Na_4Ir_3O_8$*: A Hyper-Kagome Lattice Antiferromagnet*, Phys. Rev. B **78**, 094403 (2008).
[49] J. Chaloupka, G. Jackeli, and G. Khaliullin, *Kitaev-Heisenberg Model on a Honeycomb Lattice: Possible Exotic Phases in Iridium Oxides* $A_2IrO_3$, Phys. Rev. Lett. **105**, 027204 (2010).
[50] P. Goswami, B. Roy, and S. D. Sarma, *Competing Orders and Topology in the Global Phase Diagram of Pyrochlore Iridates*, Phys. Rev. B **95**, 085120 (2017).

[51] J. M. Murray, O. Vafek, and L. Balents, *Incommensurate Spin Density Wave at a Ferromagnetic Quantum Critical Point in a Three-Dimensional Parabolic Semimetal*, Phys. Rev. B **92**, 035137 (2015).

[52] I. Boettcher and I. F. Herbut, *Anisotropy Induces Non-Fermi-Liquid Behavior and Nematic Magnetic Order in Three-Dimensional Luttinger Semimetals*, Phys. Rev. B **95**, 075149 (2017).

[53] I. Boettcher and I. F. Herbut, *Superconducting Quantum Criticality in Three-Dimensional Luttinger Semimetals*, Phys. Rev. B **93**, 205138 (2016).

[54] I. F. Herbut and L. Janssen, *Topological Mott Insulator in Three-Dimensional Systems with Quadratic Band Touching*, Phys. Rev. Lett. **113**, 106401 (2014).

[55] L. Janssen and I. F. Herbut, *Excitonic Instability of Three-Dimensional Gapless Semiconductors: Large-N Theory*, Phys. Rev. B **93**, 165109 (2016).

[56] L. Janssen and I. F. Herbut, *Phase Diagram of Electronic Systems with Quadratic Fermi Nodes in* $2 < d < 4$*:* $2 + \epsilon$ *Expansion,* $4 - \epsilon$ *Expansion, and Functional Renormalization Group*, Phys. Rev. B **95**, 075101 (2017).

[57] S. H. Curnoe, *Structural Distortion and the Spin Liquid State in* $Tb_2Ti_2O_7$, Phys. Rev. B **78**, 094418 (2008).

[58] S. Onoda and Y. Tanaka, *Quantum Melting of Spin Ice: Emergent Cooperative Quadrupole and Chirality*, Phys. Rev. Lett. **105**, 047201 (2010).

[59] S. B. Lee, S. Onoda, and L. Balents, *Generic Quantum Spin Ice*, Phys. Rev. B **86**, 104412 (2012).

[60] A. M. Hallas, J. Gaudet, and B. D. Gaulin, *Experimental Insights into Ground State Selection of Quantum XY Pyrochlores*, Annu. Rev. Condens. Matter Phys. **9**, 105 (2018).

[61] R. S. K. Mong, A. M. Essin, and J. E. Moore, *Antiferromagnetic Topological Insulators*, Phys. Rev. B **81**, 245209 (2010).

[62] G. Xu, H. Weng, Z. Wang, X. Dai, and Z. Fang, *Chern Semimetal and the Quantized Anomalous Hall Effect in* $HgCr_2Se_4$, Phys. Rev. Lett. **107**, 186806 (2011).

[63] Y.-P. Huang, G. Chen, and M. Hermele, *Quantum Spin Ices and Topological Phases from Dipolar-Octupolar Doublets on the Pyrochlore Lattice*, Phys. Rev. Lett. **112**, 167203 (2014).

[64] Y.-D. Li, X. Wang, and G. Chen, *Hidden Multipolar Orders of Dipole-Octupole Doublets on a Triangular Lattice*, Phys. Rev. B **94**, 201114 (2016).

[65] J. S. Gardner, M. J. P. Gingras, and J. E. Greedan, *Magnetic Pyrochlore Oxides*, Rev. Mod. Phys. **82**, 53 (2010).

[66] Y. Shen, Y.-D. Li, H. Wo, Y. Li, S. Shen, B. Pan, Q. Wang, H. C. Walker, P. Steffens, M. Boehm, Y. Hao, D. L. Quintero-Castro, L. W. Harriger, L. Hao, S. Meng, Q. Zhang, G. Chen, and J. Zhao, *Spinon Fermi Surface in a Triangular Lattice Quantum Spin Liquid* $YbMgGaO_4$, Nature (London) **540**, 559 (2016).

[67] Y. Li, G. Chen, W. Tong, L. Pi, J. Liu, Z. Yang, X. Wang, and Q. Zhang, *Rare-Earth Triangular Lattice Spin Liquid: A Single-Crystal Study of* $YbMgGaO_4$, Phys. Rev. Lett. **115**, 167203 (2015).

[68] J. A. M. Paddison, Z. Dun, G. Ehlers, Y. Liu, M. B. Stone, H. Zhou, and M. Mourigal, *Continuous Excitations of the Triangular-Lattice Quantum Spin Liquid* $YbMgGaO_4$, Nat. Phys. **13**, 117 (2017).

[69] Y.-D. Li, Xi. Wang, and G. Chen, *Anisotropic Spin Model of Strong Spin-Orbit-Coupled Triangular Antiferromagnets*, Phys. Rev. B **94**, 035107 (2016).

[70] J. Liu, L. Savary, T. Suzuki, J. Checkelsky, and L. Balents, *Unconventional Magnetism and Electronic Transport in Magnetic Weyl Semimetals RAlX*, Bull. Am. Phys. Soc. (2018).

[71] C. Guo, C. Cao, M. Smidman, F. Wu, Y. Zhang, F. Steglich, F.-C. Zhang, and H. Yuan, *Possible Weyl Fermions in the Magnetic Kondo System CeSb*, npj Quantum Mater. **2**, 39 (2017).

[72] H.-H. Lai, S. E. Grefe, S. Paschen, and Q. Si, *Weyl-Kondo Semimetal in Heavy-Fermion Systems*, Proc. Natl. Acad. Sci. U.S.A. **115**, 93 (2018).